Bundle formation in biomimetic hydrogels

Article

pubs.acs.org/Biomac

Bundle Formation in Biomimetic Hydrogels

Maarten Jaspers,[†] A. C. H. Pape,[‡] Ilja K. Voets,[‡] Alan E. Rowan,[*,†,§] Giuseppe Portale,[∥,⊥] and Paul H. J. Kouwer[*,†]

[†]Radboud University, Institute for Molecules and Materials, Heyendaalseweg 135, 6525 AJ Nijmegen, The Netherlands

[‡]Eindhoven University of Technology, Laboratory for Macromolecular and Organic Chemistry, and Laboratory of Physical Chemistry, and Institute for Complex Molecular Systems, P.O. Box 513, 5600 MB Eindhoven, The Netherlands

[§]The University of Queensland, Australian Institute for Bioengineering and Nanotechnology, Brisbane, Queensland 4072, Australia

[∥]Netherlands Organisation for Scientific Research (NWO), DUBBLE CRG at the ESRF, 6 rue Jules Horowitz, 38043 Grenoble Cedex, France

[⊥]University of Groningen, Department of Macromolecular Chemistry and New Polymeric Materials, Nijenborgh 4, 9747 AG Groningen, The Netherlands

Supporting Information

ABSTRACT: Bundling of single polymer chains is a crucial process in the formation of biopolymer network gels that make up the extracellular matrix and the cytoskeleton. This bundled architecture leads to gels with distinctive properties, including a large-pore-size gel formation at very low concentrations and mechanical responsiveness through nonlinear mechanics, properties that are rarely observed in synthetic hydrogels. Using small-angle X-ray scattering (SAXS), we study the bundle formation and hydrogelation process of polyisocyanide gels, a synthetic material that uniquely mimics the structure and mechanics of biogels. We show how the structure of the material changes at the (thermally induced) gelation point and how factors such as concentration and polymer length determine the architecture, and with that, the mechanical properties. The correlation of the gel mechanics and the structural parameters obtained from SAXS experiments is essential in the design of future (synthetic) mimics of biopolymer networks.

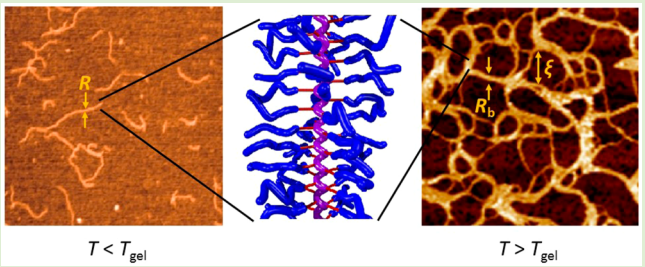

INTRODUCTION

Hydrogels find increasing use in the biomedical field, where their mechanical properties are a critical factor in many cellular processes.[1−4] A hydrogel with a biologically relevant stiffness is composed of either flexible polymer chains that are densely cross-linked[5−7] or, alternatively, a bundled network of semiflexible polymers or fibrils.[8−11] Although the stiffness of both gel types can seemingly overlap, their microstructure is vastly different. The flexible polymer gels, usually prepared at much higher polymer concentrations to obtain structural integrity, have pore sizes typically on the order of nanometers, while the pore sizes of the semiflexible networks can reach micrometers. For cell-culturing applications, a field that focuses increasingly strongly on 3D environments, mass transport becomes an important factor, and as a result, only network architectures with larger pore sizes are relevant as matrix material.[12] In addition to architecture, the mechanical properties of both network types strongly diverge under stress: Bundled biological networks commonly stiffen up at stress levels that cells exert to their direct environment;[13,14] in other words, in such fibrillar networks, cells interact with and mechanically alter their own environment.[15]

Nature is able to dynamically control and adapt the bundle lengths and diameters, but already in reconstituted biopolymer networks, the dynamics have disappeared and even reproducibility of bundle dimensions in these systems becomes challenging.[16−18] Synthetic gels that mimic the fibrillar morphology are extremely rare. Recently, we described one such mimic based on a helical ethylene-glycol-substituted polyisocyanide (PIC) and found that, indeed, its gels show (nonlinear) mechanical properties analogous to some biogels.[19,20] In addition, cell studies with peptide-decorated PIC gels as a 3D artificial extracellular matrix highlighted how important network architecture and nonlinear mechanics are for (stem) cell fate.[4]

The key to synthetically mimicking biological hydrogels is to control the bundled architecture, which, because of its high dilution, limited dimensions, and intrinsic disorder remains challenging to measure directly. Earlier, bundle dimensions of PIC hydrogels were estimated by AFM measurements, which, despite expected drying-in effects, yielded values in line with

Received: May 14, 2016
Revised: July 6, 2016
Published: July 13, 2016

DOI: 10.1021/acs.biomac.6b00703
Biomacromolecules 2016, 17, 2642−2649

results from macroscopic rheology.[19] For an in situ analysis of gel architectures, small-angle X-ray scattering (SAXS) has been shown to be a powerful tool.[21−24]

In this manuscript, we show how the architecture of PIC gels can be elucidated by SAXS studies. This synthetic model system offers the advantage of systematic structure manipulation. Experimentally, we find that at a very well-defined temperature bundles with a concentration-independent cross-sectional radius are formed. In addition, we show how changes in the polymer (contour) length influence the network morphology and, consequently, the mechanical properties. These architectural parameters are crucial in the design of next generation biogel mimics for artificial extracellular matrix or cytoskeletal materials.

EXPERIMENTAL SECTION

Sample Preparation. The PIC synthesis and characterization of the polymer length by viscometry were performed as previously described.[20,25] The polymer was dissolved in 18 MΩ cm purified water at the desired polymer concentration by stirring in a cold room at 4 °C for at least 24 h to make a polymer solution. Heating this solution above the gelation temperature leads to the formation of the PIC hydrogel.

Small-Angle X-ray Scattering. SAXS measurements were performed at the BM26B station at the European Synchrotron Radiation Facility (ESRF), Grenoble (France), particularly suited for polymers and soft matter.[26−28] X-ray radiation with a wavelength of λ = 0.1 nm was used, and the beam size at the sample was 1.3 × 0.3 mm ($H \times V$). SAXS images were recorded on a noiseless, highly sensitive solid-state Pilatus 1 M detector with a pixel size of 172 × 172 μm and an array dimension of 981 × 1043 pixels. The sample-to-detector distance was 3.5 m. The beam center and the scattering angle 2θ scale were calibrated using the position of diffraction peaks from a silver behenate standard powder. SAXS images were normalized by the primary beam intensity fluctuation, and the scattering from the background was scaled for the sample transmission prior to perform the background subtraction. Background-subtracted images have been radially integrated around the beam center using a python suite to obtain the $I(q)$ versus q profiles, where $q = 4\pi/\lambda \sin\theta$. Samples were contained in 2 mm quartz capillaries and inserted in a Linkam hot stage to control the sample temperature in the range of 5 to 50 °C. Absolute intensities were obtained using the secondary standard method with pure water.[29]

Fitting of the SAXS curves was achieved using the SASfit software.[30] The scattering of the polymer chains in solution was described using a wormlike model according to Kholodenko[31]

$$I(q) = (\Delta\rho)^2 \phi P_0(q, L, 2l_p) P_{CS}(q, R)$$

where $\Delta\rho = \rho_{polymer} - \rho_{water}$ is the electron density difference between the polymer chain and the solution, ϕ is the polymer volume fraction, L is the chain contour length, l_p is the polymer chain persistence length (half of the Kuhn length), and R is the cross-sectional radius of the polymer chain.

The scattering from the polymer network was described using a combination of the wormlike model[31] (describing the scattering from the polymer bundles) and of the Ornstein−Zernike (OZ) model[32] (describing the scattering from network heterogeneities, i.e., mesh size) according to the equation

$$I(q) = I_{bundles}(q) + I_{network}(q) = (\Delta\rho)^2 \phi P_0(q, L, 2l_{p,B}) P_{CS}(q, R_B) + \frac{I(0)}{1 + q^2 \xi_{OZ}^2}$$

where $\Delta\rho = \rho_{polymer} - \rho_{water}$ is the electron density difference between the polymer bundles and the solution, ϕ is the polymer volume fraction, L is the contour length of the bundles, $l_{p,B}$ is the persistence length of the bundle (half of the Kuhn length), R_B is the cross-sectional radius of the bundles, $I(0)$ is the forward scattering of the OZ term, and ξ_{OZ} is the correlation length of the network heterogeneities. Note that because the contour length L of the bundles is larger than the SAXS resolution, we kept L fixed at 160 nm. To reduce the number of free parameters and considering that the persistence length of the bundle is quite large and has minor effect on the model in the fitted q range, we set $l_{p,B}$ equal to 460 nm for all of the gels based on a theoretical model for semiflexible polymer networks.[19]

Microdifferential Scanning Calorimetry. Micro-DSC measurements were performed on a Multi Cell DSC (TA Instruments). The samples were loaded into the machine in the liquid state at 1 °C. The samples were heated at a rate of 0.25 °C/min to a maximum of 60 °C and subsequently cooled at a rate of 2 °C/min to a minimum of 1 °C. The heating and cooling ramps were performed twice for all samples, and all DSC measurements shown are the second heating ramps. The transition temperatures given correspond to the temperature at which a maximum in the heat capacity was reached.

Rheology. Measurements were performed on a stress-controlled rheometer (Discovery HR-1, TA Instruments) in an aluminum parallel plate geometry with a diameter of 40 mm and a gap of 500 μm. Samples were loaded into the rheometer in the liquid state at 5 °C. To determine the gelation temperature, we heated the sample at a rate of 1.0 °C/min, and the complex modulus G^* was measured by applying an oscillatory deformation of amplitude $\gamma = 0.04$ at a frequency of ω = 1.0 Hz. The gelation temperature values given correspond to the onset of the increase in the storage modulus G' relative to the baseline.

RESULTS AND DISCUSSION

The gel-forming PIC polymers are composed of a polyisocyanide backbone that is covered by ethylene glycol tails (Figure 1). The polymer length is controlled by the polymerization conditions and has a large influence on the mechanical properties in the gel phase.[20] Other methods to control gel mechanics are the polymer concentration, temperature, and the addition of different salts.[33] The triethylene glycol side chains attached to the polymer backbone render the polymer thermoresponsive. An aqueous PIC solution shows a phase transition from a low viscous solution to a transparent elastic gel when heated beyond its lower critical solution temperature (LCST).[19,34]

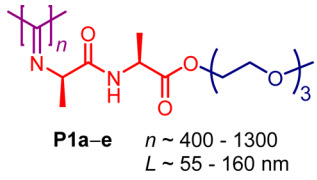

Figure 1. Molecular structure of the ethylene glycol-substituted polyisocyanides **P1a−e** with the helical polymer backbone in purple, a dipeptide substituent in red, and the triethylene glycol tail in blue. The five polymers **P1a−e** have different average chain contour lengths L, where **P1a** is shortest with L = 55 nm corresponding to $n \approx 400$ monomers and **P1e** is longest with L = 160 nm and $n \approx 1300$ monomers.

Solution Phase and Gel Phase. Gels prepared from polymers with an average contour length L = 160 nm (**P1e**), determined by viscometry measurements as previously described,[20] were studied by SAXS to determine their nanoscale architecture in situ and thus without the complications of drying-in effects. The samples were studied both in the solution phase at low temperature at T = 5 °C and in the gel phase at high temperature at T = 50 °C (see Experimental Section for details); see Figure 2. At temperatures below the gelation temperature, the polymers can be considered freely diffusing

DOI: 10.1021/acs.biomac.6b00703
Biomacromolecules 2016, 17, 2642−2649

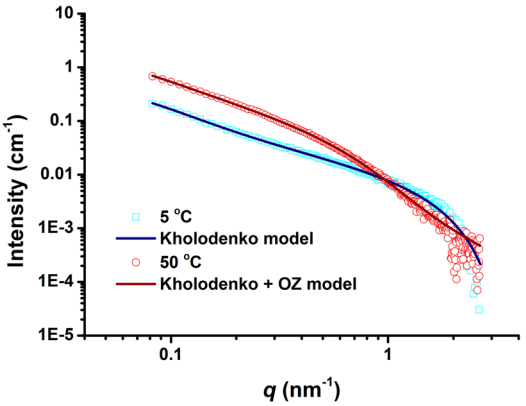

Figure 2. SAXS curves for a 5 mg mL^{-1} **P1e** sample in the liquid state at low temperature and in the gel state at high temperature. The solid lines represent the best fit to the Kholodenko model for the low-temperature data and the best fit to the composite model with a Kholodenko term and an Ornstein–Zernike term for the high-temperature data.

semiflexible chains in solution. In this solution state (Figure 2, blue squares), the SAXS data can be described by the semiflexible polymer model of Kholodenko,[31] which does not include interpolymer interactions (blue solid line). Details of the scattering model and the fitting procedures are given in the Experimental Section. In the data analysis, the average contour length L of the polymers was kept fixed at 160 nm, which is well outside the accessible range of scattering angles. We obtain both the polymer cross-sectional radius, R, and the polymer stiffness expressed as the persistence length, l_p, of a single polymer chain in solution, which are $R = 1.1 \pm 0.1$ nm and $l_p = 12 \pm 2$ nm, respectively. The latter value matches well with the l_p obtained from single-molecule force spectroscopy measurements.[19]

Upon heating the polymer solution to $T = 50$ °C, well above the gelation temperature of 19 °C of **P1e**,[20] the shape of the scattering profile (Figure 2, red circles) clearly changes compared with the low-temperature spectrum. The forward scattering intensity increases with temperature, indicating the aggregation of polymers into larger polymer bundles. These interpolymer interactions generate heterogeneities in the polymer network on larger length scales, which requires a more extensive model to describe the SAXS profiles in the hydrogel phase.[35] We find that the excess scattering intensity due to these heterogeneities can be described excellently with the model of Ornstein and Zernike.[32] Figure 2 shows the experimental scattering data at $T = 50$ °C (red circles) and a fit to the composite Kholodenko/Ornstein–Zernike (KOZ) model (red line); see also Figure S1 for the contribution of both models. From the Ornstein–Zernike term, we obtain a characteristic length scale, ξ_{OZ}, which represents the length scale of heterogeneities in the PIC network.[35]

To reduce the number of fitting parameters in the combined model, we fixed the polymer contour length $L = 160$ nm and the persistence length of the polymer bundles $l_{p,B} = 460$ nm. In the bundled network, L approaches infinity, and the persistence length was previuosly calculated[19] using a theoretical model for semiflexible networks.[36] The precise values of $l_{p,B}$ and L, however, have very little effect on the fit results. Modeling of the scattering data using these values yields a bundle cross-sectional radius $R_B = 3.0 \pm 0.2$ nm at $T = 50$ °C. This significantly larger radius compared with the liquid phase at $T =$ 5 °C confirms that the polymers are bundled in the gel phase, as was previously concluded from AFM images of dried polymer networks.[19] From the single polymer and bundle cross-sectional radii, the bundle number N (the average number of polymers per bundle) can be estimated as $N = R_B^2/R^2 = 7.3$. This bundle number corresponds remarkably well to the $N = 6.9$ that was previously determined by AFM analysis.[19] It was previously argued that this very well-defined bundle size may be related to helicity of the PICs, similar to many biopolymers.[37,38]

Concentration Dependence. If the helical structure of the PICs indeed controls N, one expects that the bundle size is independent of polymer concentration, c. We measured SAXS curves of the gel at different concentrations, despite the narrow accessible concentration range: Limited solubility prevents the preparation of samples with concentrations higher than 5 mg mL^{-1}, and gels with concentrations below 1 mg mL^{-1} scatter too weakly to record reliably.

Figure 3 shows the SAXS curves of PIC hydrogels with five different polymer concentrations at $T = 50$ °C. The scattering

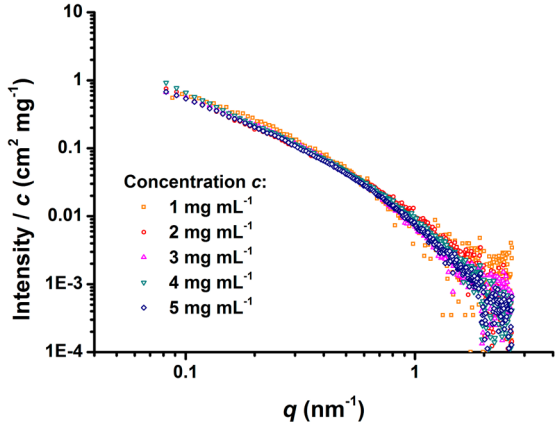

Figure 3. SAXS curves for **P1e** hydrogels at concentrations $c = 1$–5 mg mL^{-1} and temperature $T = 50$ °C. The scattering intensity is normalized by the sample concentration, yielding nearly overlapping curves. Only after fitting did small changes in the network architecture become evident.

intensity was normalized by the polymer concentration, which causes the curves to nearly superpose, indicating that the gel structure at high temperatures indeed is independent of the polymer concentration. From fitting these SAXS curves with the composite KOZ model, we find that the cross-sectional bundle radii, R_B, for all c are between 2.7 and 3.2 nm (Table 1). We anticipate that the determined length scale of heterogeneities in the PIC network ξ_{OZ}, is related to the pore size of the network. As can be expected for networks with a constant bundle size R_B, ξ_{OZ} shows a clear concentration dependence (Table 1); for gels with higher polymer concentrations, we find smaller values for ξ_{OZ}, which is in line with a denser network. Quantitatively, we find that $\xi_{OZ} \propto c^{-0.56}$ (Figure S2), which is in excellent agreement with the predicted concentration dependence of the mesh size, ξ, of the network that scales as $\xi \propto c^{-0.5}$.[13,19] This result clearly shows that despite the large distribution (in bundle dimensions and pore sizes) of the network and the low PIC concentration, we can reliably probe the architecture of the materials by SAXS.

Polymer Length Dependence. Besides the polymer concentration, the polymer contour length L has a large effect on the (nonlinear) hydrogel mechanics and the biological

DOI: 10.1021/acs.biomac.6b00703
Biomacromolecules 2016, 17, 2642–2649

Table 1. Fitting Parameters from the SAXS Data in the Gel Phase at T = 50 °C for Gels with Different Polymer Concentrations[a]

c (mg mL^{-1})	ξ_{OZ} (nm)[b]	R_B (nm)
1	76	3.2 ± 0.4
2	58	2.7 ± 0.2
3	38	3.1 ± 0.2
4	37	2.9 ± 0.1
5	30	3.0 ± 0.2

[a]Key: c is the polymer concentration of the gel; ξ_{OZ} is the length scale of heterogeneities in the PIC network that is related to the pore size; and R_B is the average bundle cross-sectional radius. [b]The error on ξ_{OZ} is difficult to determine reliably because of the small number of data points in the low q range. The error is estimated to be about half of the value of ξ_{OZ}.

function of PIC hydrogels.[4,20] Five polymers **P1a–e**, with average contour lengths ranging from 55 to 160 nm, were prepared as previously described,[20] and their SAXS profiles were measured both in the solution phase and in the gel phase. From fitting the SAXS data in the solution state with the semiflexible polymer model developed by Kholodenko,[31] we find that all five polymers have very similar cross-sectional radii, R, and persistence lengths, l_p (Table 2, Figure S3), indicating that the polymers behave very similarly in solution, independent of their contour length.

Table 2. Fitting Parameters from the SAXS Data in the Liquid Phase at T = 5 °C and the Gel Phase at T = 50 °C for Samples with Different Average Polymer Contour Lengths[a]

PIC	L (nm)	l_p (nm)	R (nm)	ξ_{OZ} (nm)[b]	R_B (nm)
P1a	55	13 ± 7	1.1 ± 0.1	>80[c]	5.0 ± 0.2
P1b	77	10 ± 1	1.1 ± 0.1	>80[c]	4.7 ± 0.2
P1c	110	9 ± 2	1.2 ± 0.1	>80[c]	3.3 ± 0.1
P1b	134	9 ± 1	1.1 ± 0.1	68	3.0 ± 0.1
P1e	160	12 ± 2	1.1 ± 0.1	30	3.0 ± 0.2

[a]Key: L is the polymer contour length as obtained from viscometry measurements (fixed during the fitting of the scattering data); l_p is the polymer persistence length; R and R_B are the cross-sectional radii of the polymer and the bundle, respectively; and ξ_{OZ} is the length scale of heterogeneities in the PIC network. Parameters l_p and R are obtained from the scattering data at T = 5 °C and ξ_{OZ} and R_B from the scattering data at T = 50 °C. [b]The error on ξ_{OZ} is difficult to determine reliably because of the small number of data points in the low q range. The error is estimated to be about half of the value of ξ_{OZ}. [c]The ξ_{OZ} values for the polymers shorter than 134 nm fall outside the range of measurable values (>80 nm).

In the gel phase at T = 50 °C, however, the SAXS curves of the gels with different polymer lengths are clearly different (Figure 4). At high scattering angles the curves seemingly superpose, but in the low q range, the scattering intensity decreases with increasing polymer length. The SAXS data were again fitted with the composite KOZ model (Figure S4), yielding ξ_{OZ} and R_B, which both show a trend with increasing polymer length (Table 2). We find that R_B changes with the polymer contour length, with shorter polymers leading to larger polymer bundles. The three longest polymers show similar bundle radii, but the two shortest polymers form larger bundles with a cross-sectional radius of ∼5 nm at T = 50 °C. This length-dependent bundling has also been observed in course-

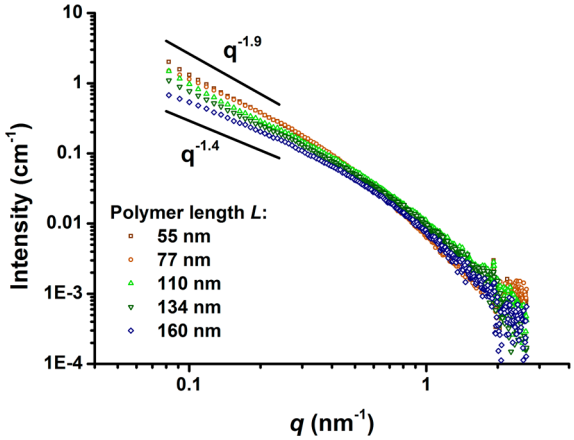

Figure 4. SAXS curves for PIC gels of **P1a–e** with different average polymer lengths at T = 50 °C and c = 5 mg mL^{-1}. The solid lines represent an $I \approx q^{-1.4}$ slope found for the longest polymer (**P1e**) and an $I \approx q^{-1.9}$ slope found for the shortest polymers (**P1a** and **P1b**).

grained simulations of semiflexible chains with a relatively simple lateral attractive potential.[39]

The network heterogeneity length scale ξ_{OZ} increases for gels of shorter polymers: 30 nm for **P1e** to 68 nm for **P1d** to much larger values for the shorter polymers (Table 2). In fact, the characteristic length scales for these polymers (ξ_{OZ} > 80 nm) are outside the accessible measurement window. The observed larger pore size of the network in combination with an identical bundle size indicates that fewer chains actively contribute to the bundled network, probably because they are too short. The relatively high molecular weight or contour length distribution of polyisocyanides (with a polydispersity index PDI = 1.3 to 1.4 for all chain lengths[20]) and the observation that very short PICs with L = 34 nm do not form gels at all[20] support this model. It also accounts for the reduced modulus that is observed for gels of short polymers.[20] Unfortunately, our current scattering setup does not allow us to accurately determine values of ξ_{OZ} for the shorter polymers.

Temperature Dependence. To study the gelation mechanism of the PIC hydrogels in more detail, we measured the SAXS profiles as a function of temperature from T = 5 to 50 °C. Figure 5a shows how the SAXS profile changes upon heating for a 5 mg mL^{-1} sample of **P1e**. The sample was incrementally heated with steps of 1 °C, and after every step the SAXS profile was measured. To prevent radiation damage to the sample, shorter exposure times of 10 s were used, which leads to noisier scattering curves, especially in the high q range. In the low q range, however, the scattering intensity clearly increases with temperature. Figure 5b shows the temperature-dependent increase in the scattering intensity at q = 0.1 nm^{-1} relative to the intensity at the lowest temperature (T = 5 °C), where the single polymers diffuse freely in solution.

At low temperatures, below 10 °C, the small-angle scattering intensity is constant, but above 10 °C the intensity increases, which is the result of the onset of bundling of the single polymers in solution. The sharpest intensity increase is observed roughly between 15 and 25 °C, which coincides perfectly with the gelation temperature, T_{gel} = 19 °C for **P1e**, as previously determined by rheology measurements.[20] At higher T, the scattering intensity shows a weaker increase with temperature. We interpret this second regime as a dehydration process, wherein more water is expelled from the bundles upon further heating. This leads to denser bundles (and a higher

DOI: 10.1021/acs.biomac.6b00703
Biomacromolecules 2016, 17, 2642–2649

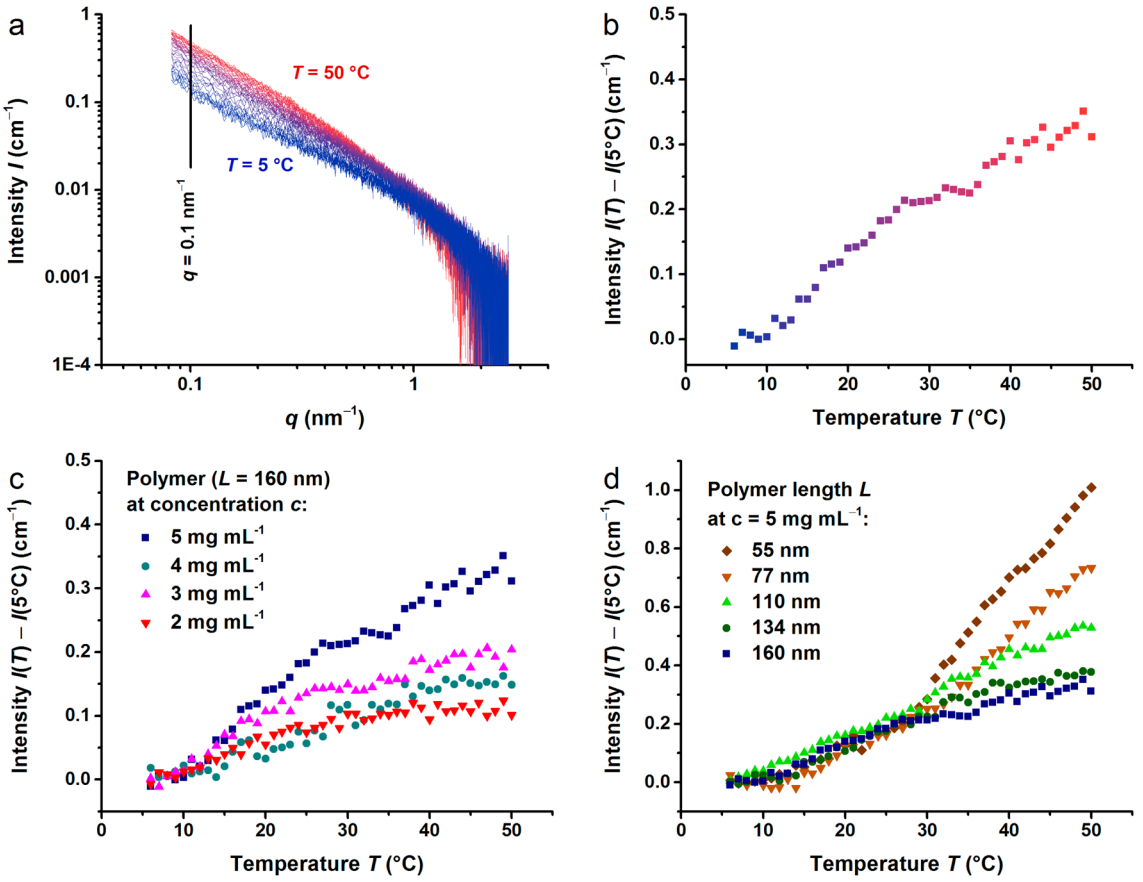

Figure 5. (a) SAXS curves measured every 1 °C from T = 5 to 50 °C for a **P1e** hydrogel with c = 5 mg mL^{-1}. The solid line represents q = 0.1 nm^{-1}. (b) Scattering intensity at q = 0.1 nm^{-1} as a function of temperature, extracted from panel a. The scattering intensity is averaged over five points around q = 0.1 nm^{-1} to reduce noise. (c) Scattering intensity at q = 0.1 nm^{-1} as a function of temperature for **P1e** gels with different polymer concentrations. (d) Scattering intensity at q = 0.1 nm^{-1} as a function of temperature for gels with different polymer lengths with c = 5 mg mL^{-1}. For both graphs the scattering intensity is averaged over five points to reduce noise.

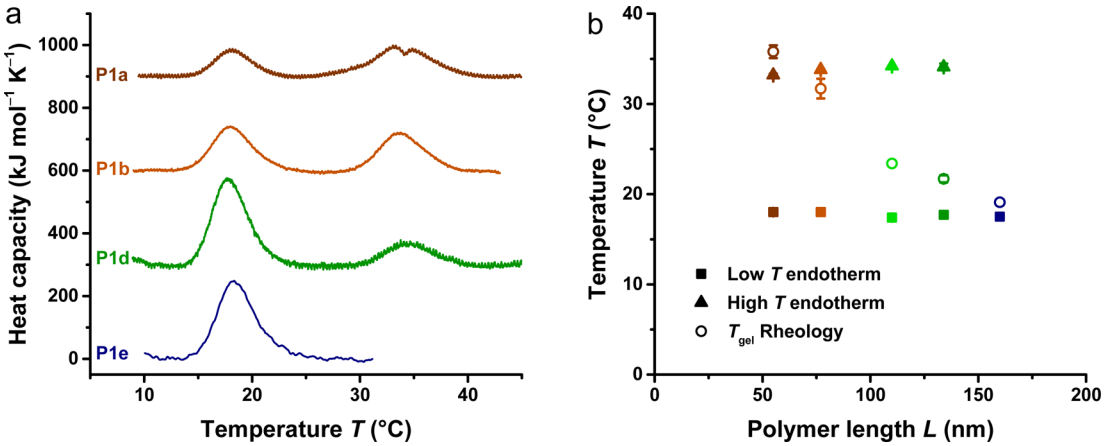

Figure 6. (a) Micro-DSC measurements of PIC hydrogels with different polymer lengths and c = 2 mg mL^{-1}. For the shorter polymers two thermal transitions are observed at very well-defined transition temperatures, while for the longest polymer only the first transition is observed. Curves have been shifted vertically for clarity. (b) Transition temperatures from micro-DSC measurements (solid symbols, taken at the maximum of the endotherm) and gelation temperature T_{gel} (open circles) for all studied polymer gels. The temperatures of the two transitions are independent of polymer length in contrast with the gelation temperature. The error bars represent standard deviations over three samples for the micro-DSC data and two samples for the rheology data.

scattering intensity) and also stiffer bundles and an increase in the storage modulus, as was experimentally observed.[19,20] Previously, a similar scenario was proposed for methylcellulose fibers, which also form strain-stiffening hydrogels upon heating,[40] and show increasing scattering intensities at higher temperatures.[41−43] Alternatively, the increase in scattering may be the result of additional polymer chains adding to the bundled architecture, although for this situation an increase in the bundle size is expected to occur simultaneously.

DOI: 10.1021/acs.biomac.6b00703
Biomacromolecules 2016, 17, 2642−2649

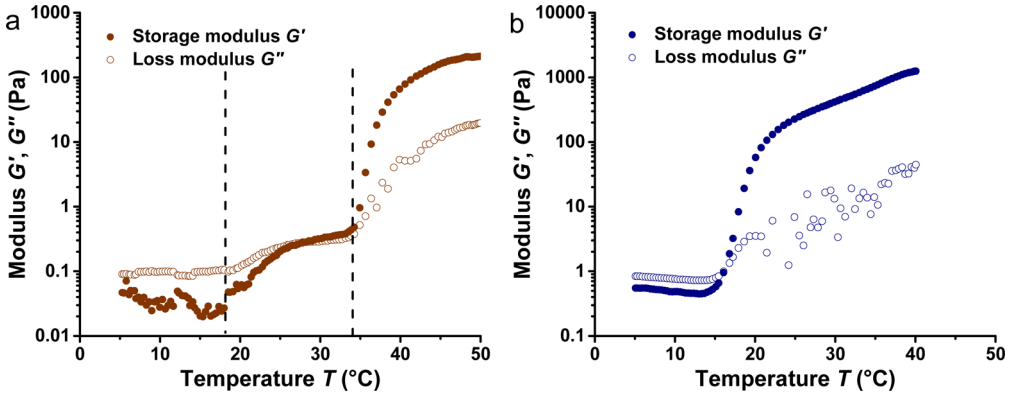

Figure 7. Storage modulus G' and loss modulus G'' as a function of temperature for (a) **P1a** and (b) **P1e** with c = 5 mg mL^{-1}. The short polymer shows two distinct transitions with gelation at the second transition, whereas the long polymer shows only a single transition. The dotted lines in panel a represent the maxima of the endotherms of the micro-DSC experiments.

The same temperature ramps were also performed for gels with lower PIC concentrations, down to 2 mg mL^{-1} (Figure 5c). Although the increase in scattering intensity as a function of T is smaller for the low concentration gels, the shape of the temperature profiles remains the same: a sharp increase in intensity up to 25 °C and a weaker increase at higher temperatures. This is once more in line with our observation that polymer bundling is independent of the polymer concentration.

When these experiments are performed on gels with different polymer lengths, however, the shape of the temperature profiles changes dramatically (Figure 5d). From T = 5 to 30 °C, the profiles of the different polymers overlap, which suggests that the initial bundling process is identical for all polymers and thus independent of the polymer contour length. Above T = 30 °C, however, the shorter polymers show a much stronger increase in scattering intensity with T than the longer polymers. We attribute this high-temperature regime to a second assembly process that predominantly occurs in the short polymer gels. This second bundling process is also responsible for the larger bundle sizes observed for the shorter polymers.

We used microdifferential scanning calorimetry (micro-DSC) to further study the thermal transitions in the gels (Figure 6). Polymer **P1e** shows a single isotherm that peaks right at the gelation temperature of the polymer, as determined by macroscopic rheology. All other shorter polymers show a second endotherm. Interestingly, for all polymer lengths, both endotherms are at exactly the same temperatures, at 18 and 34 °C, respectively. Only the relative enthalpies of the two transitions differ in size (Figure S5); the high-temperature transition dominates for the shorter polymers, and the low-temperature transition dominates for the longer polymers up to the point that the second transition completely disappears for **P1e**. The rheology-determined T_{gel} for this series follows the same line (Figure 6b): For the long polymers, it is close to the dominating first transition; for the shorter polymers it is closer to the stronger high-temperature transition. In contrast with the DSC endotherms, however, T_{gel} shows a more continuous change with polymer length. Shorter polymers probably require a higher degree of bundling to form a percolated network, which leads to a higher T_{gel} for **P1c** and **P1d** compared with the longest **P1e** polymers. The increased degree of bundling upon heating is also supported by the continuous increase in scattering intensity with temperature between roughly T = 15 and 25 °C (Figure 5).

Although **P1a** and **P1b** solutions show a transition at 18 °C and show the scattering signatures for bundling, no gel formation is observed at T < 34 °C; in other words, stress cannot percolate through the material. Most probably, the contour length of the initially formed bundles is small compared with the mesh size of the polymer network. Bundling, however, is expected to impact the rheological behavior of the (bundled) polymer solution, which indeed is observed (Figure 7a). Despite the noise at low temperature, it is clear that at T = 18 °C both G' and G'' increase, but gelation is only observed as a result of the second bundling or aggregation process at T = 34 °C, which establishes the percolated network. Consequently, the network structures of these gels are markedly different with bundles composed of (on average) 20 polymer chains and directly correlated, much larger pores. For comparison, a temperature ramp of the moduli of **P1e** in water clearly shows a single transition (Figure 7b).

CONCLUSIONS AND OUTLOOK

The aggregation of single polymer chains into bundles is a crucial process in the formation of biologically interesting hydrogels. The bundled structure leads to high persistence lengths, which gives these gels unique properties that are not observed in synthetic hydrogels composed of unbundled flexible polymer chains.

A major advantage of a bundled polymer network structure is that the minimum polymer concentration needed to form a gel with good mechanical integrity is low. For PIC and many biopolymer hydrogels, polymer concentrations as low as 0.01 wt % are sufficient,[13,19,44] while for most synthetic hydrogels minimum concentrations of at least an order of magnitude higher are required. The low polymer concentration is a direct result of the large persistence length of a polymer bundle composed of multiple much more flexible polymer chains.[19] Models show that the macroscopic stiffness of a gel $G \propto N^{3/2}$, which makes N an important parameter to optimize. An additional and intrinsic advantage of an architecture of bundled semiflexible chains is that such hydrogels show a strain-stiffening response.[14,20] Because of this stiffening response, such gels can reach a high stiffness, even at very low polymer concentrations.

Characterization of the bundled network structure is challenging, particularly because the network is dilute and relatively disorganized and polydisperse. We demonstrated that SAXS is a major tool to in situ uncover the network

DOI: 10.1021/acs.biomac.6b00703
Biomacromolecules 2016, 17, 2642−2649

architecture, and we showed how, after modeling, key network parameters and length scales can be retrieved. Integration of SAXS with additional characterization techniques, such as mechanical characterization, may provide the required insights to develop many more synthetic strain-stiffening materials in the near future.

■ ASSOCIATED CONTENT

Supporting Information

The Supporting Information is available free of charge on the ACS Publications website at DOI: 10.1021/acs.biomac.6b00703.

Additional supporting diagrams S1−S5, showing the separate contributions of both models used to fit the scattering data (Figure S1); the mesh size ξ_{OZ} as a function of polymer concentration (Figure S2); SAXS profiles of PIC solutions at T = 5 °C with different polymer lengths (Figure S3); fits for SAXS profiles of PIC gels with different polymer lengths at T = 50 °C (Figure S4); the enthalpy of transition as a function of polymer length for the two calorimetric transitions observed in micro DSC measurements (Figure S5). (PDF)

■ AUTHOR INFORMATION

Corresponding Authors

*A.E.R.: E-mail: a.rowan@science.ru.nl.
*P.H.J.K.: E-mail: p.kouwer@science.ru.nl.

Notes

The authors declare no competing financial interest.

■ ACKNOWLEDGMENTS

The ESRF and the Dutch Science Foundation (NWO) are acknowledged for providing beamtime at the Dutch-Belgian beamline (DUBBLE) for the SAXS measurements. The DUBBLE staff is acknowledged for supporting the SAXS experiments. Financial support is acknowledged from NRSCC (M.J., A.E.R.) and NanoNextNL (Grant Nos. 07A.06 and 07A.07) (A.E.R., P.H.J.K.). I.K.V was financially supported by the Dutch Science Foundation (NWO ECHO-STIP Grant 717.013.005, NWO VIDI Grant 723.014.006). This work was supported financially by the Dutch Ministry of Education, Culture and Science (Gravity program 024.001.035).

■ REFERENCES

(1) Discher, D. E.; Janmey, P.; Wang, Y. L. *Science* **2005**, *310*, 1139−1143.
(2) Engler, A. J.; Sen, S.; Sweeney, H. L.; Discher, D. E. *Cell* **2006**, *126*, 677−689.
(3) Chaudhuri, O.; Koshy, S. T.; Branco da Cunha, C. B.; Shin, J.-W.; Verbeke, C. S.; Allison, K. H.; Mooney, D. J. *Nat. Mater.* **2014**, *13*, 970−978.
(4) Das, R. K.; Gocheva, V.; Hammink, R.; Zouani, O. F.; Rowan, A. E. *Nat. Mater.* **2015**, *15*, 318−325.
(5) Naghash, H. J.; Okay, O. *J. Appl. Polym. Sci.* **1996**, *60*, 971−979.
(6) Krsko, P.; Libera, M. *Mater. Today* **2005**, *8*, 36−44.
(7) Hennink, W. E.; van Nostrum, C. F. *Adv. Drug Delivery Rev.* **2012**, *64*, 223−236.
(8) Claessens, M.; Semmrich, C.; Ramos, L.; Bausch, A. R. *Proc. Natl. Acad. Sci. U. S. A.* **2008**, *105*, 8819−8822.
(9) Pelletier, O.; Pokidysheva, E.; Hirst, L. S.; Bouxsein, N.; Li, Y.; Safinya, C. R. *Phys. Rev. Lett.* **2003**, *91*, 4.
(10) Bousquet, O.; Ma, L. L.; Yamada, S.; Gu, C. H.; Idei, T.; Takahashi, K.; Wirtz, D.; Coulombe, P. A. *J. Cell Biol.* **2001**, *155*, 747−753.
(11) Fratzl, P. *Curr. Opin. Colloid Interface Sci.* **2003**, *8*, 32−39.
(12) Baker, B. M.; Chen, C. S. *J. Cell Sci.* **2012**, *125*, 3015−3024.
(13) Gardel, M. L.; Shin, J. H.; MacKintosh, F. C.; Mahadevan, L.; Matsudaira, P.; Weitz, D. A. *Science* **2004**, *304*, 1301−1305.
(14) Storm, C.; Pastore, J. J.; MacKintosh, F. C.; Lubensky, T. C.; Janmey, P. A. *Nature* **2005**, *435*, 191−194.
(15) Jansen, K. A.; Bacabac, R. G.; Piechocka, I. K.; Koenderink, G. H. *Biophys. J.* **2013**, *105*, 2240−2251.
(16) Claessens, M.; Bathe, M.; Frey, E.; Bausch, A. R. *Nat. Mater.* **2006**, *5*, 748−753.
(17) Bruekers, S. M. C.; Jaspers, M.; Hendriks, J. M. A.; Kurniawan, N. A.; Koenderink, G. H.; Kouwer, P. H. J.; Rowan, A. E.; Huck, W. T. S. *Cell Adhesion & Migration* **2016**, 1−10.
(18) Piechocka, I. K.; Jansen, K. A.; Broedersz, C. P.; Kurniawan, N. A.; MacKintosh, F. C.; Koenderink, G. H. *Soft Matter* **2016**, *12*, 2145−2156.
(19) Kouwer, P. H. J.; Koepf, M.; Le Sage, V. A. A.; Jaspers, M.; van Buul, A. M.; Eksteen-Akeroyd, Z. H.; Woltinge, T.; Schwartz, E.; Kitto, H. J.; Hoogenboom, R.; Picken, S. J.; Nolte, R. J. M.; Mendes, E.; Rowan, A. E. *Nature* **2013**, *493*, 651−655.
(20) Jaspers, M.; Dennison, M.; Mabesoone, M. F. J.; MacKintosh, F. C.; Rowan, A. E.; Kouwer, P. H. J. *Nat. Commun.* **2014**, *5*, 5808.
(21) Cheng, X. G.; Gurkan, U. A.; Dehen, C. J.; Tate, M. P.; Hillhouse, H. W.; Simpson, G. J.; Akkus, O. *Biomaterials* **2008**, *29*, 3278−3288.
(22) Sokolova, A. V.; Kreplak, L.; Wedig, T.; Mucke, N.; Svergun, D. I.; Herrmann, H.; Aebi, U.; Strelkov, S. V. *Proc. Natl. Acad. Sci. U. S. A.* **2006**, *103*, 16206−16211.
(23) Weigandt, K. M.; Pozzo, D. C.; Porcar, L. *Soft Matter* **2009**, *5*, 4321−4330.
(24) Hirst, L. S.; Pynn, R.; Bruinsma, R. F.; Safinya, C. R. *J. Chem. Phys.* **2005**, *123*, 104902.
(25) Koepf, M.; Kitto, H. J.; Schwartz, E.; Kouwer, P. H. J.; Nolte, R. J. M.; Rowan, A. E. *Eur. Polym. J.* **2013**, *49*, 1510−1522.
(26) Borsboom, M.; Bras, W.; Cerjak, I.; Detollenaere, D.; Glastra van Loon, D.; Goedtkindt, P.; Konijnenburg, M.; Lassing, P.; Levine, Y. K.; Munneke, B.; Oversluizen, M.; van Tol, R.; Vlieg, E. *J. Synchrotron Radiat.* **1998**, *5*, 518−520.
(27) Bras, W.; Dolbnya, I. P.; Detollenaere, D.; van Tol, R.; Malfois, M.; Greaves, G. N.; Ryan, A. J.; Heeley, E. *J. Appl. Crystallogr.* **2003**, *36*, 791−794.
(28) Portale, G.; Cavallo, D.; Alfonso, G. C.; Hermida-Merino, D.; van Drongelen, M.; Balzano, L.; Peters, G. W. M.; Goossens, J. G. P.; Bras, W. *J. Appl. Crystallogr.* **2013**, *46*, 1681−1689.
(29) Orthaber, D.; Bergmann, A.; Glatter, O. *J. Appl. Crystallogr.* **2000**, *33*, 218−225.
(30) Kohlbrecher, J. *SASfit: A Program for Fitting Simple Structural Models to Small Angle Scattering Data*; Paul Scherrer Institut, Laboratory for Neutron Scattering, 2008
(31) Kholodenko, A. L. *Macromolecules* **1993**, *26*, 4179−4183.
(32) Ornstein, L. S.; Zernike, F. *KNAW Proc.* **1914**, *17*, 793−806.
(33) Jaspers, M.; Rowan, A. E.; Kouwer, P. H. J. *Adv. Funct. Mater.* **2015**, *25*, 6503−6510.
(34) Weber, C.; Hoogenboom, R.; Schubert, U. S. *Prog. Polym. Sci.* **2012**, *37*, 686−714.
(35) Di Lorenzo, F.; Seiffert, S. *Polym. Chem.* **2015**, *6*, 5515−5528.
(36) Mackintosh, F. C.; Kas, J.; Janmey, P. A. *Phys. Rev. Lett.* **1995**, *75*, 4425−4428.
(37) Grason, G. M.; Bruinsma, R. F. *Phys. Rev. Lett.* **2007**, *99*, 4.
(38) Heussinger, C.; Grason, G. M. *J. Chem. Phys.* **2011**, *135*, 035104.
(39) Pandolfi, R. J.; Edwards, L.; Johnston, D.; Becich, P.; Hirst, L. S. *Phys. Rev. E* **2014**, *89*, 062602.
(40) McAllister, J. W.; Lott, J. R.; Schmidt, P. W.; Sammler, R. L.; Bates, F. S.; Lodge, T. P. *ACS Macro Lett.* **2015**, *4*, 538−542.
(41) Kobayashi, K.; Huang, C. I.; Lodge, T. P. *Macromolecules* **1999**, *32*, 7070−7077.

DOI: 10.1021/acs.biomac.6b00703
Biomacromolecules 2016, 17, 2642−2649

(42) Lott, J. R.; McAllister, J. W.; Wasbrough, M.; Sammler, R. L.; Bates, F. S.; Lodge, T. P. *Macromolecules* **2013**, *46*, 9760−9771.
(43) Chatterjee, T.; Nakatani, A. I.; Adden, R.; Brackhagen, M.; Redwine, D.; Shen, H. W.; Li, Y. F.; Wilson, T.; Sammler, R. L. *Biomacromolecules* **2012**, *13*, 3355−3369.
(44) Piechocka, I. K.; Bacabac, R. G.; Potters, M.; MacKintosh, F. C.; Koenderink, G. H. *Biophys. J.* **2010**, *98*, 2281−2289.

DOI: 10.1021/acs.biomac.6b00703
Biomacromolecules 2016, 17, 2642−2649